

# Quantum Bayesian Inference with Renormalization for Gravitational Waves

Gabriel Escrig<sup>✉\*</sup>,<sup>1</sup> Roberto Campos<sup>✉†</sup>,<sup>1,2</sup> Hong Qi<sup>✉‡</sup>,<sup>3</sup> and M. A. Martin-Delgado<sup>✉§</sup>,<sup>1,4</sup>

<sup>1</sup>*Departamento de Física Teórica, Universidad Complutense de Madrid.*

<sup>2</sup>*Quasar Science Resources, SL.*

<sup>3</sup>*School of Mathematical Sciences, Queen Mary University of London, London E1 4NS, UK.*

<sup>4</sup>*CCS-Center for Computational Simulation, Universidad Politécnica de Madrid.*

Advancements in gravitational-wave interferometers, particularly the next generation, are poised to enable the detections of orders of magnitude more gravitational waves from compact binary coalescences. While these surges in detections will profoundly advance gravitational wave astronomy and multimessenger astrophysics, they also pose significant computational challenges in parameter estimation. We introduce a hybrid quantum algorithm *qBIRD*, which performs quantum Bayesian Inference with Renormalization and Downsampling to infer gravitational wave parameters. Testing the algorithm with both simulated and observed gravitational waves from binary black hole mergers using quantum simulators, we show that its accuracy is comparable to that of classical Markov Chain Monte Carlo methods. Our current inference runs focus on a subset of parameters, such as chirp mass and mass ratio, due to constraints from classical hardware limitations in simulating quantum algorithms. However, *qBIRD* is completely scalable, and its full potential will be unlocked when these constraints are eliminated through a small-scale quantum computer with sufficient logical qubits.

*Introduction.*—The Advanced LIGO and Advanced Virgo observatories [1, 2] have detected about 100 gravitational waves (GWs) from compact binary coalescences [3–5] since their first observation of a binary black hole (BBH) merger in 2015 [6]. A network of third-generation (3G) gravitational wave observatories, such as Cosmic Explorer (CE) [7–11], Einstein Telescope (ET) [12], and Neutron Star Extreme Matter Observatory (NEMO) [13] will significantly advance our capacity in detecting GWs, including those from compact binary coalescences, core-collapse supernovae, and rotating compact objects [14]. Consequently, GW inference will face unprecedented computational challenges [15]. Moreover, in an era of thousands of detections per day [16], the majority of the signals are overlapped. With the sensitivity improvements in low frequency band, signals can be tracked at lower frequencies and over much longer durations, extending from currently seconds to hours. These challenges cannot be easily addressed by traditional parameter estimation tools.

Quantum computing emerges as a promising solution for GW data analysis challenges, despite its rarity in gravitational-wave astronomy research. In particular, recent work has shown proof-of-principle application of a quantum algorithm in GW detection [17]. Our exploration focuses on its potential for accurate and accelerated GW inference. Quantum techniques are particularly useful for search and sampling problems [18], as shown in Fig. 1. In our previous study [19], we proved a polynomial scaling quantum advantage over classical algorithms in ranking GW likelihoods. In this work, we develop a comprehensive computational framework that implements a quantum version of the classical Markov Chain Monte Carlo (MCMC) technique [20], specifically, its archetype, the Metropolis-Hastings (MH) algorithm [21] to compute posterior probability density functions (PDFs) of GW source parameters, achieving accuracy

comparable to classical methods [22, 23]. We introduce *qBIRD*, a quantum algorithm for GW source characterization using Bayesian inference with renormalization and downsampling. We showcase the sampler’s accuracy by inferring synthetic and observed GW signals from merging BBHs.

*GW likelihood.*—For a detected gravitational wave, Bayesian inference is applied to characterize source properties. Given data  $d$  and model  $M$ , characterizing the parameter space  $\theta$  that models a gravitational wave signal  $h(\theta)$  is estimating the posterior probabilities  $p(\theta|d, M)$ . Bayes’ theorem yields these posteriors as

$$p(\theta|d, M) = \frac{\pi(\theta|M)\mathcal{L}(d|\theta, M)}{Z_M}, \quad (1)$$

where  $\pi(\theta|M)$  is the prior probability that models the belief in  $\theta$  under  $M$ ,  $\mathcal{L}(d|\theta, M)$  is the gravitational wave likelihood representing the probability of observed data  $d$  given the parameters  $\theta$  and model  $M$ , and  $Z_M = \int \mathcal{L}(d|\theta, M)\pi(\theta|M)d\theta$  is the normalization constant for the marginalized posterior likelihood, or evidence. The inference process involves computing and ranking the likelihoods between gravitational wave signals  $h(\theta)$  predicted by theory and the noisy observed data  $d$ . Since the noise is assumed to be stationary and Gaussian, and it is characterized by the power spectral density (PSD), GW likelihood follows a Gaussian about the square root of the PSD,  $S_n$ , namely,

$$\mathcal{L}(d|\theta, M) \propto \exp\left(-\sum_{i=1}^N \frac{2|d(f_i) - h(f_i; \theta)|^2}{N S_n(f_i)}\right), \quad (2)$$

where  $N$  is the total number of frequency nodes.

The GW posteriors in Eqn. (1) have two important properties for our purposes of constructing a hybrid quantum algorithm for parameter estimation based on renormalization methods (see Step 1 later): i) the GW likelihood depends solely on the disparity between

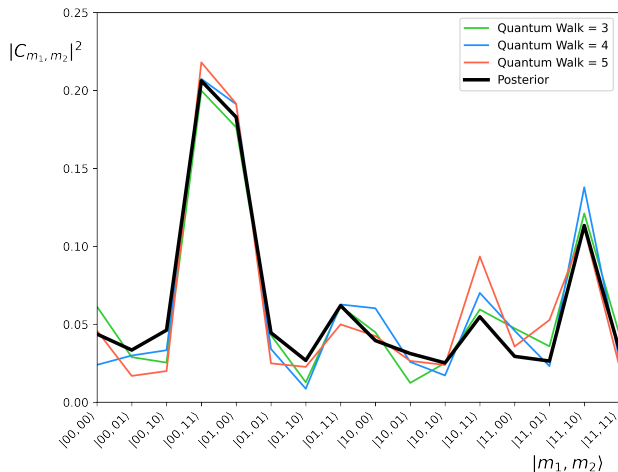


Figure 1: Discrete posterior probabilities for 16 combinations of the two component masses for GW150914 using  $Q = 2$  discretization qubits. The colored lines show the state register probabilities  $|\theta\rangle_S = |m_1, m_2\rangle_S$  for different numbers of applications of the quantum walk operator in Eqn. (5). The black line represents the posterior probabilities in Eqn. (1) for the 16 component mass combinations.

the model and observed data (S.I.1), representing pure noise (S.I.3) as long as the model aligns with the observed data, and is the product of the individual frequency bins likelihoods, and ii) the priors for source property are independent:

$$\pi(\theta|M) = \prod_{p=1}^P \pi(\theta_p|M), \quad (3)$$

with  $P$  the total number of parameters to infer. These factorization properties are the foundation for truncation (renormalization) in the quantum space of states that represent all parameters, leading to the formulation of our algorithm, which is presented and employed in the following sections.

*Quantum Metropolis algorithm.*—Parameter estimation from GW data uses stochastic sampling techniques to draw samples from the posterior distributions as described in Eqn. (1). In the GW community, this statistical analysis predominantly relies on MCMC methods [24], which demand computationally intensive numerical methods and high-performance computers. This opens the door for applying quantum algorithms developed in this work. Several approaches have been proposed to extend classical Metropolis algorithms into the quantum domain [25], showing an anticipated quantum advantage over their classical counterparts [26, 27]. In this work, we introduce a hybrid Metropolis heuristic algorithm based on quantum walks called *qBIRD*, quantum Bayesian Inference with Renormalization and Down-sampling. This approach enables the inference of source properties for gravitational waves in both observed data [28, 29] and data comprising injected waveforms into Gaussian noise, which we call injections. It not only showcases the quantum computational advantages but

also demonstrates comparable inference accuracy to classical methods [22, 23].

A quantum walk can be viewed as an agent that explores the parameter space in superposition [30], which is endowed with a quantum Hilbert space [31] of states specified as follows. Let  $\Theta$  be the configuration space of the parameters  $\theta$  we want to infer from the experimental data. The dimensionality of this space depends on the total number of parameters, about 20 for a typical binary merger event.  $\Theta$  must be discretized with a certain grid or lattice that also depends on the precision used to represent each parameter  $\theta_p$ . Our choice is a hyper-cube lattice with periodic boundary conditions that allow quantum walks between nearest-neighbor vertices.

To specify a quantum walk in this space state of parameters, we use 3 quantum registers, similar to other quantum walk proposals [27, 32]. First, a register of states  $|\theta\rangle_S$  stores the information of the parameter values. A second register  $|p\rangle_D$  encodes the hopping directions of the walker in binary notation corresponding to the oriented edges of the lattice. A third register  $|\Delta\theta\rangle_E$  stores the information of, given parameter  $\theta_p$ , moves to a neighbor site by shifting the parameter an amount  $\Delta\theta_p$  or an amount  $-\Delta\theta_p$ . Additionally, a coin state  $|\varphi\rangle_C$  accounts for the random evolution of the walker. Finally, an auxiliary register  $|A(\theta, \theta + \Delta\theta)\rangle_A$  stores the acceptance probabilities of each transition. These are given by the MH acceptance rule:

$$A(\theta, \theta + \Delta\theta) = \min\left[1, \frac{\pi(\theta + \Delta\theta)}{\pi(\theta)} \left(\frac{\mathcal{L}(d|\theta + \Delta\theta)}{\mathcal{L}(d|\theta)}\right)^\beta\right], \quad (4)$$

where  $\beta$  represents an annealing schedule.

The quantum walk employs a total of  $PQ + \lceil \log_2 P \rceil + a + 2$  qubits:  $PQ$  represents the number of qubits needed for the register  $|\theta\rangle_S$  that contains all the points of the lattice  $\Theta$ , where  $P$  is the number of inferred parameters and  $Q$  is the number of discretization qubits, with  $2^Q$  states represented for each parameter;  $\lceil \log_2 P \rceil$  qubits to represent the register  $|p\rangle_D$  in binary encoding;  $a$  qubits to represent the auxiliary register for acceptance probability. Finally, 2 qubits are needed, one for the register  $|\Delta\theta\rangle_E$ , and another for the coin register  $|\varphi\rangle_C$  to encode the accept/reject probability of all states.

Now, the evolution operator  $W$  of the quantum walk is constructed over the previous registers as follows (see S.II for its detailed construction):

$$W = RV^\dagger B^\dagger SFBV. \quad (5)$$

This enables the construction of the one-step circuit of the quantum walk, with  $W$  as a building block of a quantum MH algorithm. By applying several  $W$ 's consecutively, a quantum walk traverses the parameter space  $\Theta$  according to certain transition probabilities, just as the classical MH does. The operator  $W$  samples the posterior distribution in Eqn. (1), storing it as state probabilities, as shown in Fig. 1. The crucial aspect underpinning the superiority of the quantum algorithm over its classical counterpart lies in that each measurement simulates the

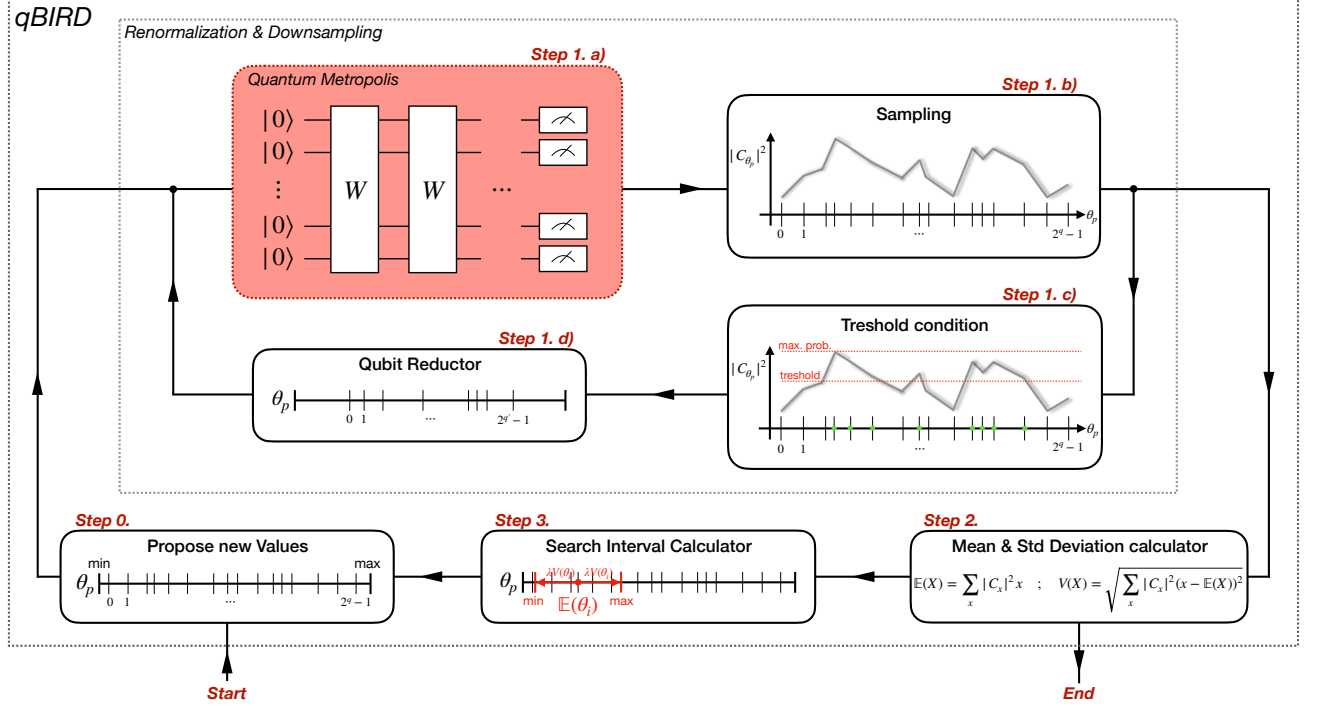


Figure 2: Flowchart of  $qBIRD$  algorithm. See main text for module and step explanations.

probability of accepting each state, capitalizing on the efficiency of superposition. Prior research demonstrated that the quantum MH algorithm achieved a polynomial scaling advantage over its classical counterpart [19].

*qBIRD algorithm.*—Using the above quantum walk as a core, we have developed a hybrid algorithm capable of inferring the posterior probability-density functions of the source parameters from gravitational wave radiation obtained from BBHs merger events, and can be used for any type of GW source.  $qBIRD$  consists of three modules: the quantum Metropolis module, the renormalization and downsampling module, and a classical postprocessing module. The description of the algorithm is as follows, and is illustrated schematically in Fig. 2.

**Step 0. Parameter initialization:** The algorithm is initialized by proposing  $2^Q$  values for each parameter, drawn from a uniform distribution specified by the lower and upper bounds of the prior function (3). All these values are stored in the state register  $|\theta\rangle_S$  producing an initial state  $|\phi^{(0)}\rangle$ .

**Step 1. Renormalization & Downsampling:** This first module executes the quantum Metropolis algorithm of (5) and is adapted from [33] and endowed with a renormalization method that defines the  $qBIRD$  algorithm. In this step, the quantum walk will be applied several times as we decrease the parameter space  $\Theta$  to locate the set of values for each parameter  $\theta_p$  maximizing the likelihood.

**a) Quantum Metropolis:** Iteratively apply the walk operator (5)  $L$  times on the initial state, which contains

$|S| := s = PQ$  qubits:

$$|\psi(L)\rangle := W_L \dots W_2 W_1 |\phi^{(0)}\rangle. \quad (6)$$

The integer  $s$  is also used as the index of the renormalization module step.

**b) Sampling:** Sample the state register  $|\theta\rangle_S$

$$|\theta\rangle_S := \sum_{x \in \Theta(s)} C_x |x\rangle_S, \quad (7)$$

from  $|\theta\rangle_S$  measurements to obtain the pairs  $\{|C_x|^2, x\}_s$ .  $\Theta(s)$  denotes the state space of qubits at the  $s$ -th step of the renormalization procedure to be described in d).

**c) Threshold condition:** If  $s = P$ , jump to Step 2, otherwise calculate the number of elements  $|S_h(s)|$  with:

$$S_h(s) := \left\{ y \in \Theta(s) : |C_y|^2 \geq \alpha \max_{x \in \Theta(s)} |C_x|^2 \right\}, \quad (8)$$

where  $\alpha \in [0, 1]$  represents a threshold and  $S_h(s)$  is a sieve to obtain it.

**d) Qubit reductor:** Reduce the number of qubits in the state register  $|\theta\rangle_S$  by defining

$$s' := \max[P, \min(|\log_2 |S_h(s)||, s - P)], \quad (9)$$

and go to Step 1a) with  $s'$  qubits and the  $2^{s'}$  highest probability values. This condition allows us to eliminate at least one qubit for each parameter, ending up with a minimum of one qubit per parameter.

The second module arises from the challenge of using the quantum Metropolis algorithm to search for the

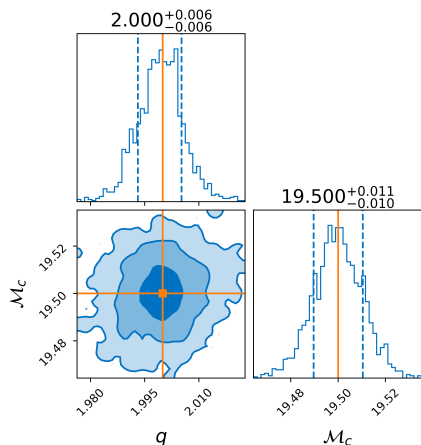


Figure 3: Posterior distributions obtained with  $qBIRD$  for the chirp mass  $\mathcal{M}_c$  and mass ratio  $q$  of a simulated BBH gravitational wave signal injected into Gaussian-noise using *PyCBC*. The injected values are  $\mathcal{M}_c = 19.5 M_\odot$  and  $q = 2$ , shown in orange.

state with the maximum probability and is inspired by the renormalization techniques of quantum lattice models [34]. Due to the enormous size of the state space, the normalization factor of quantum states results in very small probability differences between the most and least probable states. Although the probability disparity between states may span a couple of orders of magnitude, obtaining significance would require an impractical number of measurements. During the discretization process, the evidence in (1) is proportional to the size of the lattice,  $Z_M \propto |\Theta|$ . Then, as we increase the size of the parameter space  $\Theta$ , the closer to zero the probabilities will be. It is important to note that this problem is specific to Bayes' theorem and has not been introduced by using quantum computing. However, if we gradually remove the states that are significantly less probable by reducing the size and qubits of the problem, these differences become progressively more noticeable. With this technique, we are able to find the state with the maximum likelihood over all the proposed values.

The effectiveness of the quantum renormalization method in computing the maximum likelihood shown in Eqn. (1) lies in the well-suited truncations in Hilbert space of states for uncorrelated noise (Gaussian) describing the likelihood (2) and the BH parameters (3), as exemplified by properties i) and ii) after Eqn. (2).

**Step 2. Mean & Std Deviation calculator:** The third module consists of a classical processing that takes the results obtained in the first two modules to generate PDFs for each parameter and converge the algorithm. Thus, given the pairs,  $\{|C_x|^2, x\}_{s=P}$  compute:

$$\mathbb{E}(\theta_p) := \sum_{x \in \theta_p(s=P)} |C_x|^2 x, \quad (10)$$

$$V(\theta_p) := \sqrt{\sum_{x \in \theta_p(s=P)} |C_x|^2 (x - \mathbb{E}(\theta_p))^2}, \quad (11)$$

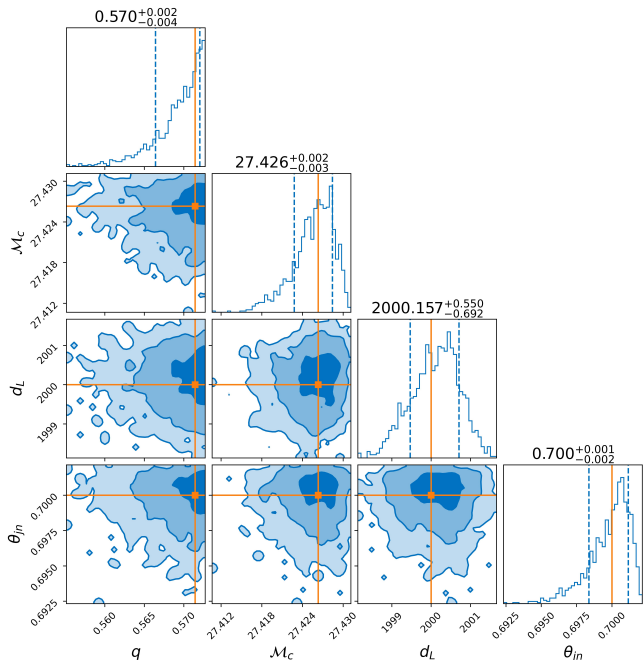


Figure 4: Posterior distributions obtained with  $qBIRD$  for a synthetic BBH signal characterized with 4 unknown parameters. The simulated gravitational wave was injected into zero-noise using *Bilby*, and the injected values are  $\mathcal{M}_c = 27.426 M_\odot$ ,  $q = 0.571$ ,  $d_L = 2000$  Mpc, and  $\theta_{jn} = 0.7$ , shown in orange.

which represent the mean and weighted standard deviation for each parameter  $p = 1, \dots, P$ , respectively. It is important to save the  $\mathbb{E}(\theta_p)$  values in each iteration in order to build the PDFs at the end of the algorithm.

**Step 3. Search interval calculator:** To gradually narrow down the search area, a new interval for each parameter is proposed from  $\mathbb{E}(\theta_p)$  and  $V(\theta_p)$  previously obtained, with lower and upper values given by:

$$\theta_{p,(\min, \max)} = \mathbb{E}(\theta_p) \mp \lambda V(\theta_p), \quad (12)$$

where  $\lambda$  is a parameter to be set for controlling the convergence of the algorithm. Note that the proposed new minimum (maximum) cannot be lower (greater) than the one set by prior interval (3). Then return to Step 0 with the new interval  $[\mathbb{E}(\theta_p) - \lambda V(\theta_p), \mathbb{E}(\theta_p) + \lambda V(\theta_p)]$ .

**End.** After a given number of iterations of Steps 0 – 3, PDFs of each of the parameters  $\theta_p$  are constructed from the  $\mathbb{E}(\theta_p)$  values obtained in each iteration.

*Results.*—We applied  $qBIRD$  to analyze two simulated GWs and compare our recovered posteriors with the known injected parameter values. One simulated GW has two parameters and the other has 4 parameters, constructed using *Bilby* [23] with a Gaussian noise and *PyCBC* [35] with a zero noise, respectively. This choice represents the current compromise between the largest possible parameter size and the capabilities of the quantum simulator [36] on a classical computer used to obtain

the inference results, compared to simulations of the LVK collaborations obtained using HPC resources [37].

Fig. 3 shows the 2-parameter inference results with  $qBIRD$  for the chirp mass  $\mathcal{M}_c$  and mass ratio  $q$  of a Gaussian-noise BBH injection realized using  $PyCBC$ . The priors for this inference are  $\mathcal{M}_c \in [19.4, 19.6] M_\odot$  and  $q \in [1.9, 2.1]$ , using  $Q = 6$  discretization qubits and 2000 iterations.  $qBIRD$  accurately and precisely recovered the injected values  $\mathcal{M}_c = 19.5 M_\odot$  and  $q = 2$ , which fall within the 90% confidence intervals of the inferred posteriors, respectively. The slight derivations in the peak values from the injected ones and the small measurement uncertainties of the two injected values were caused by the Gaussian noise.

As a more demanding inference, Fig. 4 shows the posterior distributions of the 4-parameter estimation of the chirp mass  $\mathcal{M}_c$ , mass ratio  $q$ , luminosity distance  $d_L$ , and inclination angle  $\theta_{jn}$  of the zero-noise BBH injection generated using  $Bilby$ . In this inference, the priors are  $\mathcal{M}_c \in [27.41, 27.44] M_\odot$ ,  $q \in [0.545, 0.575]$ ,  $d_L \in [1997, 2002] \text{ Mpc}$ , and  $\theta_{jn} \in [0.690, 0.705]$ . Due to the limitations of the classical simulators, the discretization qubits had to be reduced to  $Q = 3$  and done with 1300 iterations. Although the inference was significantly overcomplicated, the  $qBIRD$  algorithm was still able to reproduce the injected values  $\mathcal{M}_c = 27.426 M_\odot$ ,  $q = 0.571$ ,  $d_L = 2000 \text{ Mpc}$  and  $\theta_{jn} = 0.7$ . This figure illustrates the scalability potential of  $qBIRD$  in estimating more parameters in the inference process.

In SM S.IV, more technical details are provided for Figs. 3 and 4. and refer for more inference cases. Further, we applied  $qBIRD$  algorithm for a few more GWs, one injection into zero-noise and one in observed data, shown in S.III. Moreover, correct scalability with increasing number of parameters has been verified, approaching the limit of quantum simulators. It is crucial to emphasize that this limitation stems from classical simulators, and the algorithm exhibits full scalability when a robust quantum environment becomes feasible.

*Conclusions.*—We have introduced our hybrid quantum algorithm,  $qBIRD$ , for GW parameter estimation, showcasing its accuracy using the parameter estimation runs for the 2-parameter and the 4-parameter simulated gravitational waves from BBH mergers. It builds upon the QMS framework [33] that was tested with a scaling advantage [19]. It introduces renormalization and

downsampling techniques with quantum walks to realize a quantum version of the classical MCMC sampler. The posterior distributions inferred using  $qBIRD$  are accurate and consistent with the results obtained using classical computing methods. The increased uncertainties in the 4-parameter case compared to the 2-parameter case are mainly due to the small number of discretization qubits and the fewer iterations. Classical simulators are inherently limited in the size of circuits that can be run, and the same is true for current quantum hardware. However, since  $qBIRD$  is fully scalable, it will benefit from the upward trend of quantum advances in the near term.

*Acknowledgments.*—G.E., R.C. and M.A.M.-D. acknowledge the support from grants MINECO/FEDER Projects, PID2021-122547NB-I00 FIS2021, MADQuantumCM project funded by Comunidad de Madrid, the Recovery, Transformation, and Resilience Plan, NextGenerationEU, funded by the European Union, and the Ministry of Economic Affairs Quantum ENIA project funded by Madrid ELLIS Unit CAM. M.A.M.-D. has also been partially supported by the U.S. Army Research Office through Grant No.W911NF-14-1-0103. This work used the computing facilities of the GICC group at UCM. H.Q. thanks Frank Linde for inspiring her quantum computing exploration for gravitational wave data analysis in 2021 summer. H.Q. extends gratitude to Louisiana State University and LIGO Livingston Observatory for their hospitality during this work in 2023. H.Q. was supported in part by the 2022-2023 additional STFC IAA grant to Queen Mary University of London. H.Q. is grateful for computational resources provided by LIGO Laboratory and the Leonard E Parker Center for Gravitation, Cosmology and Astrophysics at the University of Wisconsin-Milwaukee and supported by National Science Foundation Grants PHY-0757058, PHY-0823459, PHY-1626190, and PHY-1700765. In part the computing resources at Queen Mary University of London were supported by QMUL’s 2023 STFC IAA award. This material is based upon work supported by NSF’s LIGO Laboratory which is a major facility fully funded by the National Science Foundation. G.E. and R.C. equally contributed to this work.

\* gescrig@ucm.es

† robecamp@ucm.es

‡ hong.qi@ligo.org

§ mardel@ucm.es

- 
- [1] J. Aasi *et al.* (LIGO Scientific), *Class. Quant. Grav.* **32**, 074001 (2015), arXiv:1411.4547 [gr-qc].
- [2] F. Acernese *et al.* (VIRGO), *Class. Quant. Grav.* **32**, 024001 (2015), arXiv:1408.3978 [gr-qc].
- [3] B. P. Abbott *et al.* (LIGO Scientific, Virgo), *Phys. Rev. X* **9**, 031040 (2019), arXiv:1811.12907 [astro-ph.HE].
- [4] R. Abbott *et al.* (LIGO Scientific, Virgo), *Phys. Rev. X* **11**, 021053 (2021), arXiv:2010.14527 [gr-qc].
- [5] R. Abbott *et al.* (KAGRA, VIRGO, LIGO Scientific), *Phys. Rev. X* **13**, 041039 (2023), arXiv:2111.03606 [gr-qc].
- [6] B. P. Abbott *et al.* (LIGO Scientific Collaboration and Virgo Collaboration), *Phys. Rev. Lett.* **116**, 061102 (2016).
- [7] S. Dwyer, D. Sigg, S. W. Ballmer, L. Barsotti, N. Mavalvala, and M. Evans, *Phys. Rev. D* **91**, 082001 (2015).
- [8] R. Essick, S. Vitale, and M. Evans, *Phys. Rev. D* **96**, 084004 (2017).



- [9] K. Chamberlain and N. Yunes, *Phys. Rev. D* **96**, 084039 (2017).
- [10] E. D. Hall *et al.*, *Phys. Rev. D* **103**, 122004 (2021), arXiv:2012.03608 [gr-qc].
- [11] M. Evans *et al.*, (2021), arXiv:2109.09882 [astro-ph.IM].
- [12] Punturo1, M. et al., *Classical and Quantum Gravity* **27**, 8 (2010).
- [13] K. Ackley *et al.*, *Publ. Astron. Soc. Austral.* **37**, e047 (2020), arXiv:2007.03128 [astro-ph.HE].
- [14] V. Kalogera *et al.*, (2021), arXiv:2111.06990 [gr-qc].
- [15] P. Couvares *et al.*, (2021), arXiv:2111.06987 [gr-qc].
- [16] I. Gupta *et al.*, (2023), arXiv:2307.10421 [gr-qc].
- [17] S. Gao, F. Hayes, S. Croke, C. Messenger, and J. Veitch, *Phys. Rev. Res.* **4**, 023006 (2022).
- [18] D. Hangleiter and J. Eisert, *Reviews of Modern Physics* **95**, 035001 (2023).
- [19] G. Escrig, R. Campos, P. A. M. Casares, and M. A. Martin-Delgado, *Class. Quantum Gravity* **40**, 045001 (2023).
- [20] M. van der Sluys, V. Raymond, I. Mandel, C. Röver, N. Christensen, V. Kalogera, R. Meyer, and A. Vecchio, *Classical and Quantum Gravity* **25**, 184011 (2008).
- [21] N. Christensen, R. Meyer, and A. Libson, *Class. Quantum Gravity* **21**, 317 (2004).
- [22] S. A. Usman, A. H. Nitz, I. W. Harry, C. M. Biwer, D. A. Brown, M. Cabero, C. D. Capano, T. Dal Canton, T. Dent, S. Fairhurst, *et al.*, *Classical and Quantum Gravity* **33**, 215004 (2016).
- [23] G. Ashton, M. Hübner, P. D. Lasky, C. Talbot, K. Ackley, S. Biscoveanu, Q. Chu, A. Divakarla, P. J. Easter, B. Goncharov, *et al.*, *The Astrophysical Journal Supplement Series* **241**, 27 (2019).
- [24] N. Christensen and R. Meyer, *Rev. Mod. Phys.* **94**, 025001 (2022).
- [25] K. Temme, T. J. Osborne, K. G. Vollbrecht, D. Poulin, and F. Verstraete, *Nature* **471**, 87 (2011).
- [26] M.-H. Yung and A. Aspuru-Guzik, *Proceedings of the National Academy of Sciences* **109**, 754 (2012), <https://www.pnas.org/doi/pdf/10.1073/pnas.1111758109>.
- [27] J. Lemieux, B. Heim, D. Poulin, K. Svore, and M. Troyer, *Quantum* **4**, 287 (2020).
- [28] PyCBC, “Data used of 4-OGC,” <https://github.com/gwastro/4-ogc/tree/master/posterior> (2022).
- [29] LIGO, “Data of event for GW events,” <https://dcc.ligo.org/public/> (2016), [Online; accessed January-2024].
- [30] D. Aharonov, A. Ambainis, J. Kempe, and U. Vazirani, in *Proceedings of the thirty-third annual ACM symposium on Theory of computing* (2001) pp. 50–59.
- [31] M. Szegedy, in *45th Annual IEEE symposium on foundations of computer science* (IEEE, 2004) pp. 32–41.
- [32] K. Miyamoto, *Physical Review Research* **5** (2023), 10.1103/PhysRevResearch.5.033059.
- [33] R. Campos, P. A. M. Casares, and M. A. Martin-Delgado, *Quantum Machine Intelligence* **5** (2023), 10.1007/s42484-023-00119-y.
- [34] K. G. Wilson, *Reviews of modern physics* **47**, 773 (1975).
- [35] A. Nitz, I. Harry, D. Brown, C. M. Biwer, J. Willis, T. D. Canton, C. Capano, T. Dent, L. Pekowsky, G. S. C. Davies, S. De, M. Cabero, S. Wu, A. R. Williamson, B. Machenschalk, D. Macleod, F. Pannarale, P. Kumar, S. Reyes, dfinstad, S. Kumar, M. Tápai, L. Singer, P. Kumar, veronica villa, maxtrevor, B. U. V. Gadre, S. Khan, S. Fairhurst, and A. Tolley, “gwastro/pycbc: v2.3.3 release of pycbc,” (2024).
- [36] M. S. ANIS *et al.*, “Qiskit: An open-source framework for quantum computing,” (2021).
- [37] P. Canizares, S. E. Field, J. Gair, V. Raymond, R. Smith, and M. Tiglio, *Physical review letters* **114**, 071104 (2015).
- [38] A. H. Nitz, S. Kumar, Y.-F. Wang, S. Kastha, S. Wu, M. Schäfer, R. Dhurkunde, and C. D. Capano, *The Astrophysical Journal* **946**, 59 (2023).
- [39] A. H. Nitz, S. Kumar, Y.-F. Wang, S. Kastha, S. Wu, M. Schäfer, R. Dhurkunde, and C. D. Capano, *Astrophys. J.* **946**, 59 (2023).

— Supplementary Materials —

## Quantum Bayesian Inference with Renormalization for Gravitational Waves

Gabriel Escrig, Roberto Campos, Hong Qi, and M. A. Martin-Delgado

### Appendix S.I: Likelihood calculation

In General Relativity (GR), GWs are described by perturbations  $h_{\mu\nu}$  of the spacetime metric as  $ds^2 = (\eta_{\mu\nu} + h_{\mu\nu})dx^\mu dx^\nu$ , where  $\eta_{\mu\nu}$  is the flat Minkowski reference metric. In the transverse-traceless (TT) gauge, there are only 2 independent transversal polarization modes denoted as  $h_+$  and  $h_\times$ . The main goal of current GW detectors such as LIGO, Virgo, and KAGRA is to retrieve information on compact object coalescences from acquired data  $d(t)$  during  $t = 1, 2, \dots, T$  data collection intervals. These data represent an observation of an event that may correspond to a binary black hole merger. To establish such correspondence, a model  $M$  from GR is needed to represent the merger. When the model is faithful enough, we can obtain very useful information about intrinsic parameters of the colliding BHs such as their masses  $m_1, m_2$ , spins  $s_1, s_2$  or extrinsic parameters such as their positions in the sky.

A model  $M$  representing a GW signal is denoted by  $h(t; \boldsymbol{\theta})$  where  $\boldsymbol{\theta}$  are the parameters characterizing the gravitational wave. This modeled signal is confronted with the experimental data  $d(t)$ . The model is considered faithful when the difference from the data and the signal is pure noise, namely, uncorrelated Gaussian noise  $n(t)$ :

$$d(t) - h(t; \boldsymbol{\theta}) = n(t). \quad (\text{S.I.1})$$

The signal  $h(t)$  is a function of the two polarizations  $h_+(t), h_\times(t)$ , and the antenna patterns  $F_+, F_\times$ ,

$$h(t) = F_+ h_+(t) + F_\times h_\times(t). \quad (\text{S.I.2})$$

Antenna patterns depend on the detector geometry and encode the effect of the extrinsic parameters.

In the frequency domain  $f_i$ , with  $i = 1, 2, \dots, T$ , this noise is characterized through the PSD,  $S_n$ , in the noise correlation function:

$$n(f_i)n(f_j) = \frac{T}{2} S_n(f_i) \delta_{ij}, \quad (\text{S.I.3})$$

where  $n(f_i)$  is the transformed noise distribution and  $T$  the elapsed detection time.

From the statistical analysis of the data it is possible to estimate the values of the source parameters using Bayesian inference. Describing the parameter space  $\boldsymbol{\theta}$  with respect to the given data  $d(f_i)$  and the model  $M$  involves the use of PDFs denoted as  $p(\boldsymbol{\theta}|d, M)$ . Then, the inference of GW parameters proceeds by introducing the posterior probability by the Bayes theorem (1).

### Appendix S.II: Quantum Walk Operator Construction

The quantum walk operator  $W = RV^\dagger B^\dagger SFBV$  (5) is composed of the following elementary operations. It starts by making a superposition over all possible movements with the  $V$  operator:

$$V |0\rangle_D |0\rangle_E = \frac{1}{\sqrt{2p}} \sum_{i=0}^{p-1} |i\rangle_D \sum_{j \in \{0,1\}} |j\rangle_E = \frac{1}{\sqrt{2p}} [|0\rangle_D + |1\rangle_D + \dots + |p-1\rangle_D] \otimes [|0\rangle_E + |1\rangle_E]. \quad (\text{S.II.1})$$

It is implemented by applying Hadamard gates to all qubits. Once all possible moves are in superposition, the acceptance probabilities (4) are encoded into the coin register with the  $B$  operator:

$$B |\boldsymbol{\theta}\rangle_S |i\rangle_D |\Delta\boldsymbol{\theta}_i\rangle_E |A(\boldsymbol{\theta}, \boldsymbol{\theta} + \Delta\boldsymbol{\theta}_i)\rangle_A |\varphi\rangle_C = |\boldsymbol{\theta}\rangle_S |i\rangle_D |\Delta\boldsymbol{\theta}_i\rangle_E |A(\boldsymbol{\theta}, \boldsymbol{\theta} + \Delta\boldsymbol{\theta}_i)\rangle_A \mathcal{U}(\vartheta) |\varphi\rangle_C, \quad (\text{S.II.2})$$

where  $\Delta\boldsymbol{\theta}_i = (0, 0, \dots, \overset{\text{parameter } i}{\Delta\theta}, \dots, 0)$ , each element of the vector being a specific parameter. Implementing this operator consists of a rotation  $\mathcal{U}(\vartheta)$  of angle  $\vartheta = \arcsin\left(\sqrt{A(\boldsymbol{\theta}, \boldsymbol{\theta} + \Delta\boldsymbol{\theta}_i)}\right)$  controlled by the  $|A(\boldsymbol{\theta}, \boldsymbol{\theta} + \Delta\boldsymbol{\theta}_i)\rangle_A$  register.

At this point, the transition in the state register  $|\theta\rangle_S$  is performed by the  $F$  operator:

$$F|\theta\rangle_S|i\rangle_D|\Delta\theta_i\rangle_E|\varphi\rangle_C = \begin{cases} |\theta\rangle_S|i\rangle_D|\Delta\theta_i\rangle_E|0\rangle_C & \text{if } |\varphi\rangle_C = |0\rangle_C, \\ |\theta + \Delta\theta_i\rangle_S|i\rangle_D|\Delta\theta_i\rangle_E|1\rangle_C & \text{if } |\varphi\rangle_C = |1\rangle_C. \end{cases} \quad (\text{S.II.3})$$

and can be constructed from an adder gate conditioned by the coin register  $|\varphi\rangle_C$ . Then, the operator  $S$  flips the sign of the value in the register  $|\Delta\theta_i\rangle_E$  conditioned by the coin register  $|\varphi\rangle_C$ :

$$S|\theta\rangle_S|i\rangle_D|\Delta\theta_i\rangle_E|\varphi\rangle_C = \begin{cases} |\theta\rangle_S|i\rangle_D|\Delta\theta_i\rangle_E|0\rangle_C & \text{if } |\varphi\rangle_C = |0\rangle_C, \\ |\theta\rangle_S|i\rangle_D|-\Delta\theta_i\rangle_E|1\rangle_C & \text{if } |\varphi\rangle_C = |1\rangle_C. \end{cases} \quad (\text{S.II.4})$$

and can be constructed from a CNOT gate controlled by the coin register  $|\varphi\rangle_C$ . Finally, the changes in the movement and coin registers are reversed and then the  $|0\rangle_P|0\rangle_E|0\rangle_C$  state is subject to the following reflection with the  $R$  operator defined as follows:

$$R|i\rangle_D|\Delta\theta_i\rangle_E|\varphi\rangle_C = \begin{cases} -|0\rangle_D|0\rangle_E|0\rangle_C & \text{if } (i, \Delta\theta_i, \varphi) = (0, \mathbf{0}, 0), \\ |i\rangle_D|\Delta\theta_i\rangle_E|\varphi\rangle_C & \text{otherwise.} \end{cases} \quad (\text{S.II.5})$$

### Appendix S.III: Extra results for qBIRD inferences

Apart from the results obtained in the main text, it can be seen that  $qBIRD$  is able to perform different types of inference, among which real data are highlighted. This section is devoted to this purpose. Technical details of the inferences can be found in S.IV.

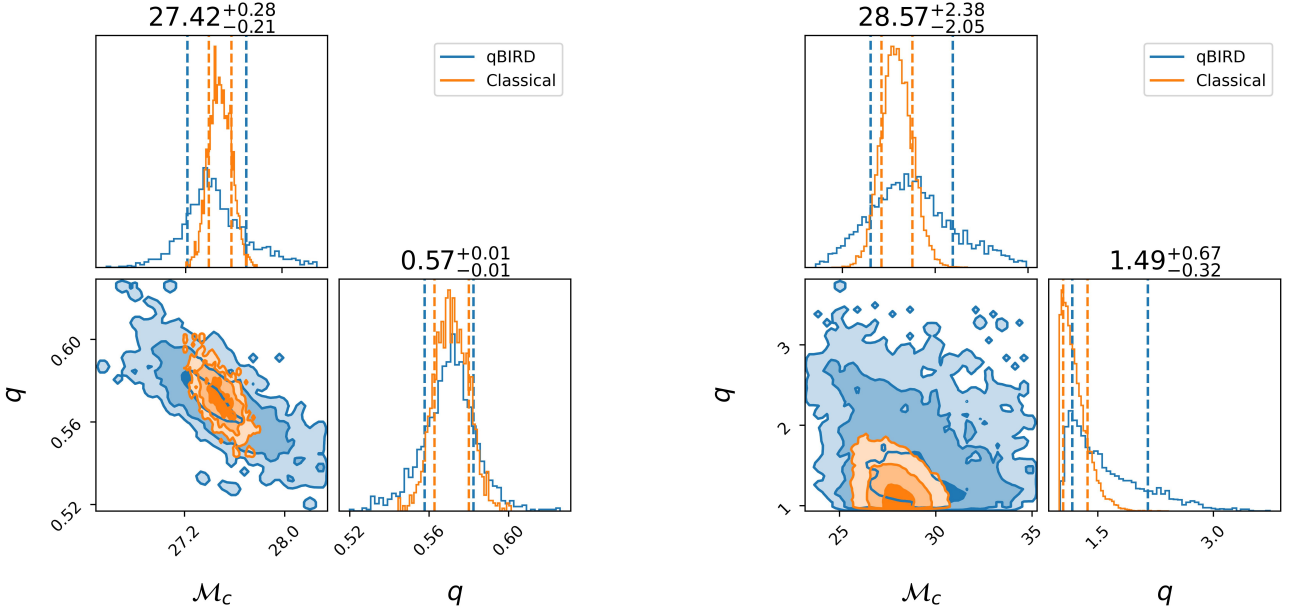


Figure S1: Corner plots of the PDFs obtained by  $qBIRD$  for the chirp mass  $\mathcal{M}_c$  and mass ratio  $q$  for: (Left) a zero-noise BBH injection, compared to the inference of the GW library *Bilby*, (Right) the first detected BBH event, GW150914, compared to the GW catalog [38] from *PyCBC*.



### Appendix S.IV: Technical details for qBIRD inferences

Fig. 3 represents the posteriors obtained by *qBIRD* for the chirp mass  $\mathcal{M}_c$  and the mass ratio  $q$  of a simulated gaussian-noise BBH injection, calculated with the GW library *PyCBC*. The injection values for these inference are  $\mathcal{M}_c = 19.5 M_\odot$  and  $q = 2$ . The prior is set uniform to the intervals  $\mathcal{M}_c \in [19.4, 19.6] M_\odot$  and  $q \in [1.9, 2.1]$ . Regarding the technical details of the *qBIRD* inference, the PDFs are constructed from 2000 iterations with a discretization of  $Q = 6$  qubits per parameter. This implies splitting the sample space of each parameter into  $2^6$  points, yielding to  $2^{12}$  possible configurations for  $P = 2$  parameters. In addition,  $a = 3$  qubits were used for the ancilla register, in total 18 qubits to execute the circuit. The quantum circuit has executed 4 steps  $W$  in each iteration with a constant annealing schedule of  $\beta = 0.5$ .

Fig. 4 represents the posteriors obtained by *qBIRD* of a 4-parameter inference of a simulated zero-noise BBH injection, calculated with the GW library *Bilby*. The parameters inferred are the chirp mass  $\mathcal{M}$ , the mass ratio  $q$ , the luminosity distance  $d_L$  and the inclination angle  $\theta_{jn}$ . The injection values for these inference are  $\mathcal{M}_c = 27.426 M_\odot$ ,  $q = 0.571$ ,  $d_L = 2000$  Mpc and  $\theta_{jn} = 0.700$ . The prior is set uniform to the intervals  $\mathcal{M}_c \in [27.41, 27.44] M_\odot$ ,  $q \in [0.545, 0.575]$ ,  $d_L \in [1997, 2002]$  Mpc and  $\theta_{jn} \in [0.690, 0.705]$ . Regarding the technical details of the *qBIRD* inference, the PDFs are constructed from 1300 iterations with a discretization of  $Q = 3$  qubits per parameter. This implies splitting the sample space of each parameter into  $2^3$  points, yielding to  $2^{12}$  possible configurations for  $P = 4$  parameters. In addition,  $a = 3$  qubits were used for the ancilla register, in total 18 qubits to execute the circuit. The quantum circuit has executed 4 steps  $W$  in each iteration with a constant annealing schedule of  $\beta = 50$ .

Fig. S1 (left) represents the posteriors obtained by *qBIRD* for the chirp mass  $\mathcal{M}_c$  and the mass ratio  $q$  of a simulated zero-noise BBH injection, calculated with the GW library *Bilby* and superimposed, classical results obtained by a classical MCMC *Bilby* sampler. The injection values for these inference are  $\mathcal{M}_c = 27.43 M_\odot$  and  $q = 0.57$ . The prior is set uniform to the intervals  $\mathcal{M}_c \in [25, 100] M_\odot$  and  $q \in [0.25, 1]$ . Regarding the technical details of the *qBIRD* inference, the PDFs are constructed from 1500 iterations with a discretization of  $Q = 5$  qubits per parameter. In addition,  $a = 3$  qubits were used for the ancilla register, in total 16 qubits to execute the circuit. The quantum circuit has executed 4 steps  $W$  in each iteration with a constant annealing schedule of  $\beta = 500$ . Classical inference has been performed with the same number of points, using the same injection values and priors with the *bilby\_mcmc* sampler.

Fig. S1 (right) represents the posteriors obtained by *qBIRD* for the chirp mass  $\mathcal{M}_c$  and the mass ratio  $q$  of the real BBH event GW150914 extracted from official LIGO repositories data and superimposed, classical results obtained by the *PyCBC* catalog inference [39] to show the quality of the quantum inference. Regarding the technical details of the *qBIRD* inference, the PDFs are constructed from 1500 iterations with a discretization of  $Q = 5$  qubits per parameter. In addition,  $a = 3$  qubits were used for the ancilla register, in total 16 qubits to execute the circuit. The quantum circuit has executed 4 steps  $W$  in each iteration with a constant annealing schedule of  $\beta = 0.5$ .

Some technical information of the *qBIRD* algorithm is summarized in Table S1.

Table S1: Technical details of the inferences in Figures 3, 4 and S1. All quantum inferences have been generated with 4 steps of  $W$  in each iteration with a constant annealing schedule and with  $a = 3$  ancilla qubits.

Inference	Injection Values	Prior intervals	Disc. Qubits	$\beta$ Schedule	Iterations
Fig. 3	$\mathcal{M}_c = 19.5 M_\odot, q = 2$	$\mathcal{M}_c \in [19.4, 19.6] M_\odot, q \in [1.9, 2.1]$	$Q = 6$	$\beta = 0.5$	2000
Fig. 4	$\mathcal{M}_c = 27.426 M_\odot, q = 0.571,$ $d_L = 2000$ Mpc, $\theta_{jn} = 0.7$	$\mathcal{M}_c \in [27.41, 27.44] M_\odot, q \in [0.545, 0.575],$ $d_L \in [1997, 2002]$ Mpc, $\theta_{jn} \in [0.690, 0.705]$	$Q = 3$	$\beta = 50$	1300
Fig. S1 (Left)	$\mathcal{M}_c = 27.43 M_\odot, q = 0.57$	$\mathcal{M}_c \in [25, 100] M_\odot, q \in [0.25, 1]$	$Q = 5$	$\beta = 500$	1500
Fig. S1 (Right)	-	$\mathcal{M}_c \in [23, 42] M_\odot, q \in [1, 4]$	$Q = 5$	$\beta = 0.5$	1500